PTEP

Prog. Theor. Exp. Phys. **2016**, 053D01 (15 pages)
DOI: 10.1093/ptep/ptw041

Deuteron-like neutron–proton correlation in ^{18}F studied with the cluster-orbital shell model approach

Hiroshi Masui[1,*] and Masaaki Kimura[2,3]

[1]*Information Processing Center, Kitami Institute of Technology, Kitami 090-8507, Japan*
[2]*Department of Physics, Faculty of Science, Hokkaido University, Sapporo 060-0810, Japan*
[3]*Nuclear Reaction Data Centre, Faculty of Science, Hokkaido University, Sapporo 060-0810, Japan*
*E-mail: hgmasui@mail.kitami-it.ac.jp

Received November 3, 2015; Revised March 20, 2016; Accepted March 22, 2016; Published May 21, 2016

We study the deuteron-like correlation ($T = 0$) in ^{18}F using the cluster-orbital shell model approach within the core $+p + n$ model space, which successfully reproduces the observed properties of ^{18}F such as $B(M1)$ and the matter radius. Based on the analysis of the correlation energy, magnetic moment, and opening angle, it is found that the deuteron-like proton–neutron pair is formed despite the deep binding of the valence nucleons. It is shown that the $[j_> \otimes j_<]^{J=1}_{T=0}$ configurations play an important role because of the deuteron-like pair formation. We show that the strong correlation leads to the non-negligible occupation of pf and higher shells that are embedded in the single-particle continua, and gives rise to the spatially correlated deuteron-like pair formation. We also investigate how the spin–orbit interaction affects the correlation energy, because the occupation probability of the $[j_> \otimes j_<]^{J=1}_{T=0}$ configurations strongly depends on the spin–orbit splitting.

Subject Index D11

1. Introduction

Nuclear force is more attractive in isoscalar ($T = 0$) channels than in isovector ($T = 1$) channels, yielding a bound state. Nevertheless, much less is known about the formation of $T = 0$ nucleon pairs in a finite nucleus, and it remains a longstanding problem [1–3], while the $T = 1$ pair condensate is well known. One reason for this situation is the lack of experimental examples. In ordinary stable $N \neq Z$ nuclei, the $T = 0$ pair formation is trivially suppressed, since protons and neutrons around the Fermi surface occupy different single-particle orbits.

Currently, interest in the $T = 0$ pairing is strong, because modern radioactive-isotope-beam experimental facilities provide a unique opportunity to verify the $T = 0$ pair formation and condensate in stable and unstable $N = Z$ nuclei up to $A \simeq 100$ systems, in which valence protons and neutrons occupy the same major shell. It has been pointed out that the $[j_1 \otimes j_2]^J_T = [\, j_> \otimes j_<]^1_0$ configuration, where $j_{\gtrless} \equiv \ell \pm 1/2$ denote the spin–orbit partners belonging to the same major shell, plays a central role in $T = 0$ pair formation, and hence the large spin–orbit splitting between the $j_>$ and $j_<$ orbits prevents the pair formation [2,4,5]. In other words, we can expect $T = 0$ pair formation and condensation if certain conditions are satisfied, i.e., the spin–orbit splitting is small, and both $j_{\gtrless}$ orbits are not Pauli-blocked. Indeed, a strong $T = 0$ neutron–proton correlation has been reported in ^{18}F and ^{42}Sc [5], where the $j_{\gtrless}$ orbits are unblocked and fully available for the valence neutron and

proton. The large contribution of the $[j_> \otimes j_<]^1_0$ component has been discussed within the sd-shell model space [6–10]. In heavy nuclei, for which the spin–orbit splitting is expected to be small, the $T = 0$ pair condensate and mixed-pair condensate have also been discussed [11,12].

Knowing the good possibility of $T = 0$ pair formation in certain nuclei, e.g., in ^{18}F, the following question naturally arises: "Is a strongly correlated and spatially localized neutron–proton pair formed or not?"; more specifically, "Does a (quasi-)bound deuteron-like pair exist in a finite nucleus?" This is an analogous question to di-neutron (proton) formation and Bose–Einstein condensate–Bardeen–Cooper–Schrieffer (BCS) crossover phenomena discussed for $T = 1$ pairs [13–15]. Many studies have been devoted to investigating the properties of $T = 0$ nucleon pairs. For example, the quasi-deuteron configurations in odd–odd $N = Z$ nuclei were investigated in Ref. [16], and, more recently, the mixing of single-particle orbits with even and odd orbital angular momenta, which give rise to the spatially localized pair formation in ^{18}F, was investigated [17]. Our study shares the aim of those preceding studies. We examine how $[j_> \otimes j_<]$-type coupling such as the $[d_{5/2} \otimes d_{3/2}]^1_0$ configuration and the spin–orbit splitting affect $T = 0$ pair formation and its spatial localization in ^{18}F by means of the ^{16}O+p+n three-body model.

As is already known for the $T = 1$ pair cases [18], the mixing of single-particle states with even and odd orbital angular momenta is essential for the spatially correlated and localized pair formation, because it breaks the symmetry of the parity in the body-fixed frame. In the case of the nucleons above the ^{16}O core, the lowest two single-particle states, $0d_{5/2}$ ($l = 2$) and $1s_{1/2}$ ($l = 0$), are bound and have an even number of orbital angular momenta. However, the $0d_{3/2}$ state, which is the spin–orbit partner of $0d_{5/2}$, and other higher orbital states with odd orbital angular momenta are all unbound and embedded in the single-particle continua. Therefore, an appropriate theoretical approach that can properly describe both the bound and unbound states is indispensable. For this purpose, we employ the cluster-orbital shell model approach [19]. By using the ^{16}O+N potential that reproduces the bound and unbound states of ^{17}O and ^{17}F [29], we have investigated the structure of the ground and excited 0^+ states. It is found that, in the 1^+ ground state, the proton and neutron pair gains a large amount of the correlation energy and forms a spatially localized deuteron-like pair despite the deep binding. Because of this spatial correlation, it is shown that the $[j_> \otimes j_<]^{J=1}_{T=0}$ configurations and single-particle continua play important roles. The dependence of the spin–orbit splitting is also discussed.

The paper is organized as follows. In Sect. 2, the formalism of our calculation and potential for the ^{16}O+N system and for valence nucleons are explained. In Sect. 3, we present the calculated results for 1^+ and 0^+ states of ^{18}F. We show that the $[j_> \otimes j_<]$ configuration triggers the strong $T = 0$ pair correlation and the contribution from the single-particle continua, giving rise to the formation of the spatially correlated deuteron-like pair. We also examine how the $T = 0$ pair formation is affected by the spin–orbit splitting. In Sect. 4, the summary and discussion are given.

2. Model and formalism

To study ^{18}F in an ^{16}O+p+n three-body model, we employ the cluster-orbital shell model (COSM) approach [19]. In COSM, the coordinates ($\boldsymbol{r}_1$ and $\boldsymbol{r}_2$) are spanned from the center of mass of the core nucleus to valence nucleons, as illustrated in Fig. 1. The Hamiltonian of COSM, in which the center-of-mass motion is subtracted, is formulated as follows:

$$\hat{H} = \sum_{i=1}^{2} \left(\hat{t}_i + \hat{v}_i^{\mathrm{CN}} \right) + \left(\hat{T}_{12} + \hat{V}_{12} \right), \tag{1}$$

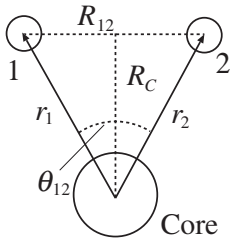

Fig. 1. Definitions of the coordinates in COSM ($\boldsymbol{r}_1$ and $\boldsymbol{r}_2$) and other quantities, R_{12}, R_C, and θ_{12}.

where $\hat{t}_i$ and $\hat{v}_i^{\rm CN}$ are the kinetic and potential energy operators for the ith valence nucleon. In the second parentheses of Eq. (1), $\hat{T}_{12} = \boldsymbol{p}_1 \cdot \boldsymbol{p}_2 / M_C$ is the recoil term coming from the subtraction of the center-of-mass motion due to the finite mass M_C of the core nucleus. $\hat{V}_{12}$ is a two-body interaction between valence nucleons.

We prepare the basis functions of COSM in the following way. The basis function ϕ_{α_i} for the ith valence particle is defined by applying the Gaussian expansion method (GEM) [20–22] to the radial part as follows:

$$\phi_{\alpha_i}(\boldsymbol{r}_i) = N_i r_i^{\ell_i} \exp\left(-\tfrac{1}{2} a_i r_i^2\right) [\ell_i \otimes s_i]_{j_i m_i} \ \chi^{\tau}_{m_{t_i}}. \tag{2}$$

Here, N_i is the normalization factor, and α_i denotes a set of the parameters of the basis function $\{a_i,\ j_i, \ell_i,\ m_i,\ m_{t_i}\}$. The range parameter a_i in ϕ_{α_i} is discretized in the geometrical progression manner as

$$a_i = b_0 \gamma^{q-1} \quad (q = 1, 2, \ldots, q_{\rm max}). \tag{3}$$

In this calculation, we apply $b_0 = 0.1$ fm, $\gamma = 1.25$, and $q_{\rm max} = 20$.

The COSM basis function for the two-valence-nucleon system is prepared in the jj-coupling scheme using ϕ_α as follows:

$$\Phi_{\alpha_1\alpha_2} \equiv \mathcal{A}\left\{\left[\phi_{\alpha_1} \otimes \phi_{\alpha_2}\right]^{JM}_{TM_T}\right\}, \tag{4}$$

where $\mathcal{A}$ is the antisymmetrizer for particles 1 and 2. The eigenstates of the Hamiltonian, $\hat{H}\Psi_k = E_k \Psi_k$, are described by the expansion with $\Phi_{\alpha_1\alpha_2}$ as follows:

$$\Psi_k = \sum_{\alpha_1\alpha_2} C^{(k)}_{\alpha_1\alpha_2} \Phi_{\alpha_1\alpha_2}. \tag{5}$$

It has been shown that the COSM approach with GEM correctly takes the continuum contributions into the model space [22,23] and yields the same numerical result as the Gamow shell model (GSM) [24–27] approach in the study of ^{4}He+2n(2p) systems [28].

In this work, we use the same interaction as applied in Refs. [29–31] for the $^{16}{\rm O} + N$ part $\hat{v}_i^{\rm CN}$, which is constructed in a semi-microscopic procedure by folding the density of the core and taking into account the exchange effect with the valence particles [32]. The potential consists of three terms as follows:

$$\hat{v}_i^{\rm CN} \equiv \hat{v}_i^{\rm fold} + \hat{v}_i^{LS} + \hat{\Lambda}_i \quad (i = 1, 2). \tag{6}$$

The first term $\hat{v}_i^{\rm fold}$ is the central potential, which is constructed by applying the folding procedure with the core density, and the knock-out exchange diagram is also taken into account [32]:

$$\begin{aligned}\hat{v}_i^{\rm fold}|\Psi_{\rm valence}\rangle &\equiv \langle \Psi_{\rm core}| \sum_m \hat{v}_{im} |\mathcal{A}'\{\Psi_{\rm core} \cdot \Psi_{\rm valence}\rangle\}\rangle \\ &= \hat{v}_i^{\rm d} + \hat{v}_i^{\rm ex}. \end{aligned} \tag{7}$$

Table 1. Calculated energies of ^{17}O and ^{17}F using the ^{16}O+N potential [29] compared with the experimental values [36]. All units are in MeV. Numbers in parentheses are total decay widths in MeV.

	State	Theory	Experiment [36]
^{17}O	$5/2^+$	-4.19	-4.14
	$1/2^+$	-3.28	-3.27
	$3/2^+$	0.95	0.94
		($\Gamma = 0.14$)	($\Gamma = 0.096$)
	$7/2^-$	9.21	–
		($\Gamma = 6.04$)	–
	$5/2^-$	10.44	–
		($\Gamma = 13.40$)	–
	w/o LS ($\ell = 2$)	-1.78	–
^{17}F	$5/2^+$	-0.61	-0.60
	$1/2^+$	-0.14	-0.11
	$3/2^+$	3.89	4.40
		($\Gamma = 0.96$)	($\Gamma = 1.53$)
	$7/2^-$	12.17	–
		($\Gamma = 7.68$)	–
	$5/2^-$	13.14	–
		($\Gamma = 15.51$)	–
	$3/2^-$	2.50	–
		($\Gamma = 7.12$)	–
	w/o LS ($\ell = 2$)	1.55	–
		($\Gamma = 0.04$)	–

Here, the antisymmetrizer $\mathcal{A}'$ expresses the exchange of two nucleons, one in the core and the other from the valence nucleons. $\hat{v}_i^{\rm d}$ and $\hat{v}_i^{\rm ex}$ are the direct and exchange parts. For the second term $\hat{v}_i^{LS}$, we introduce an effective spin–orbit potential as $\hat{v}_i^{LS} = V_{LS}^0 f_{LS}(r_i/b)(\boldsymbol{L}_i \cdot \boldsymbol{S}_i)$, where the radial part is taken as $f_{LS}(x) \equiv (2x^2 - 1)\exp(-x^2)$. The potential parameters are the same as those applied in the study of oxygen isotopes [29], adjusted to reproduce the spin–orbit splitting of the low-lying positive-parity states of ^{17}O as $5/2^+$ and $3/2^+$: $V_{LS}^0 = 97.5$ MeV and $b = 1.723$ fm. The third term is introduced in order to eliminate the Pauli-forbidden states in the relative motion between the ^{16}O core and a valence nucleon. To this end, we apply the orthogonality condition model (OCM) [33]. For practical calculations of OCM, we introduce a projection operator to the Pauli-forbidden state $|FS\rangle$ as

$$\hat{\Lambda}_i = \lambda |FS\rangle\langle FS|. \tag{8}$$

By taking $\lambda \to \infty$ in the diagonalization, the forbidden states are eliminated from the physical solutions [34]. The Pauli-forbidden states in ^{16}O ($0s_{1/2}$, $0p_{3/2}$, and $0p_{1/2}$ states) are expressed by the harmonic oscillator wave functions with the size parameter $b = 1.723$ fm, which is adjusted to the matter radius of ^{16}O.

This ^{16}O+N potential reproduces the energy of the $5/2^+$, $1/2^+$, and $3/2^+$ states in ^{17}O and ^{17}F, as summarized in Table 1. The f-wave states, $7/2^-$ and $5/2^-$, are obtained as resonant states with large imaginary parts in the complex eigenenergies. Here, the complex eigenenergies of the resonant states are obtained by applying the complex scaling method [21,22,35]. For the p-wave, we can only obtain the $3/2^-$ resonant pole in ^{17}F with the complex energy of 2.50–i3.56 (MeV). Other p-wave resonances, $1/2^-$ in ^{17}F, $3/2^-$ and $1/2^-$ in ^{17}O, are not obtained within a reasonable numerical stability, since the imaginary part becomes very large compared to the real part. We have calculated

the location of these poles by changing the attraction of the potential and followed the trajectory of the poles. It is confirmed that the real parts of the poles are at most a few MeV, and the imaginary part is at least twice as large as the real one.

We have checked the dependence of the results on the definition of the Pauli-forbidden states $|FS\rangle$ in Eq. (8). If we use the eigenstates of the core–N potential, $\hat{v}_i^{\rm fold} + \hat{v}_i^{LS}$, instead of the harmonic oscillator wave functions, the result can be changed. However, it is found that the change can be considered to be rather small; e.g., the position of the $1p_{3/2}$ pole is changed from 2.50–i3.56 to 2.42–i3.55 (MeV), and hence the dependence of the definition of $|FS\rangle$ is rather minor. This is because of the large overlap between the harmonic oscillator wave function and the eigenstates with the $\hat{v}_i^{\rm fold} + \hat{v}_i^{LS}$ potential, which amounts to 0.992, 0.983, 0.987 for the $0s_{1/2}$, $0p_{3/2}$, $0p_{1/2}$ states, respectively.

In the three-body calculation, the unbound-state contributions are treated on the same footing as the bound states in the framework of the GEM. As shown in Refs. [22,23,28], the continuum contributions of the single-particle states are correctly taken into account. For the two-body interaction of the valence nucleons $\hat{V}_{12}$ in Eq. (1), we apply an effective nucleon–nucleon interaction, the Minnesota potential [37], with an exchange parameter of $u = 1.0$. In the present calculation of ^{18}F, we adjusted the strength of the $T = 0$ and 1 channels. Details of this adjustment are given in the following sections.

3. Results and discussions

3.1. Energy levels and physical quantities of ^{18}F

We calculate the energies of ^{18}F in our ^{16}O+p+n three-body model with the maximum angular momentum of the partial waves as $\ell_{\rm max} = 6$. The original strength of the Minnesota potential for the valence nucleons gives a large binding energy for the 1^+ ($T = 0$) state of $E_B = 12.03$ MeV compared to the observed value, 9.75 MeV. The excitation energies of the $T = 1$ states (0^+ and 2^+) are also overestimated using the original strength of the Minnesota potential, as shown in the left-hand part of Fig. 2. Hence, in order to reproduce the binding energy and excitation levels, we multiply the isospin-dependent factors 0.80 ($T = 0$) and 1.40 ($T = 1$) by the original Minnesota potential. The obtained energy levels are shown in the middle part of Fig. 2. The overall agreement between the calculation and experiment is improved; in particular, the energy gap between the 1^+ and 0^+ states shows good agreement with the experiment. Therefore, we use this choice of potential parameters in the following discussions.

The convergence of the energy in the $T = 0$ and $T = 1$ channels with respect to the maximum angular momentum of the partial waves is shown in Figs. 3(a) and (b). As an illustration of the spatial localization of valence nucleons, we also calculate the opening angle θ_{12}, which is calculated as $\theta_{12} = 2\tan^{-1}(R_{12}/2R_C)$. Here, R_{12} and R_C are defined in Fig. 1. From Fig. 3(a), we can see a clear difference in the model-space dependence between the $1^+(T = 0)$ and $0^+(T = 1)$ states. The energy of the 0^+ state, which only includes the $(\ell_j)^2$-type components in the jj-coupling scheme, converges very quickly at $\ell_{\rm max} = 3$. It can also be seen in the calculation of the opening angle, as shown in Fig. 3(b). This indicates that the valence proton and neutron are coupled with a BCS-like pair, which has the same spin and opposite z-component, and the jj-coupling scheme can describe the wave function of the valence nucleons correctly.

On the other hand, the convergence of the 1^+-state energy is slow with respect to the increase of the maximum angular momentum. A similar behavior of the convergence has been discussed in weakly bound Borromean nuclei such as ^{6}He and ^{11}Li. It is known that, if the model space is defined in the

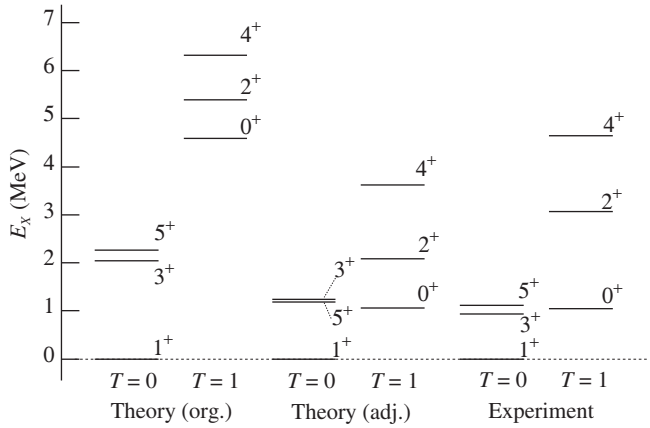

Fig. 2. Calculated and experimental [38] excitation energies of ^{18}F measured from the 1^+_1 ($T = 0$) state. In the theoretical calculations, "(org.)" shows the calculation with the original strength of the Minnesota potential, and "(adj.)" means the calculation with an adjusted strength. For the strength parameters, please see the text.

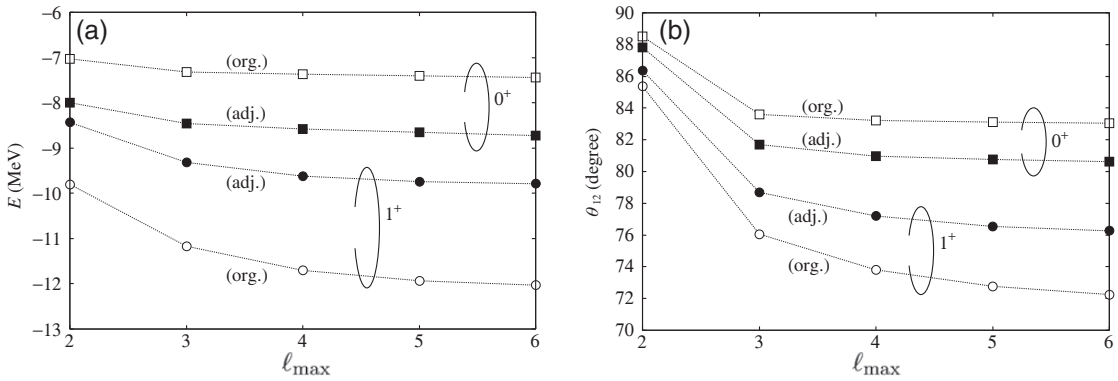

Fig. 3. $\ell_{\max}$ dependence of the energy and opening angle in ^{18}F. Solid and open symbols are calculations using the ^{16}O+N potential with the original and adjusted strengths, respectively. Circles are for the 1^+ state, and squares are for the 0^+ state.

shell-model-like picture, i.e., the jj-coupling scheme, the convergence of the calculation becomes very slow [43]. Generally, for such weakly bound systems in which the interactions of the core–N and N–N are of the same order of magnitude and the binding energy is small (less than 1 MeV), the three-body model treatment is suitable to describe the correlation of the valence nucleons. Judging from the binding energy of the 1^+ state in ^{18}F, which is more than ten times higher than the ^{6}He and ^{11}Li cases, the jj-coupling scheme treatment is considered to be sufficient to describe the 1^+ state. However, the slow convergence of the energy of the 1^+ state indicates that the correlation of the valence nucleons is strong, and the LS-coupling scheme treatment is necessary for the 1^+ state.

The $M1$ transition strength $B(M1; 0^+_1 \to 1^+_1)$ is a good benchmark to examine the wave functions of the 1^+ and 0^+ states. The experiments report a very large $M1$ strength of $B(M1) = 19.71\,\mu_N^2$ [39]. In Ref. [16], the single-j model space calculation, where only the $[d_{5/2} \otimes d_{5/2}]$ configurations are taken into account, was applied and yielded an $M1$ strength of $B(M1) = 15.18\,\mu_N^2$, which reaches about three-quarters of the observed value. Our calculation gives a larger $M1$ transition strength of $B(M1) = 18.30\,\mu_N^2$, which is shown in the third column of Table 2 and almost reproduces the experiment. This result shows that the change in the coupling scheme induces the enhancement of

Table 2. $M1$ transition strengths, magnetic moments, r.m.s. radii, mean distances of the valence nucleons, and opening angles for the 1^+ state of ^{18}F. For details, see text.

	Theory: 1^+ (org.)	(adj.)	Theory: 0^+ (org.)	(adj.)	Experiment: 1^+
$B(M1; 0^+ \to 1^+)$ (μ_N^2)	16.83	18.30	–	–	19.71 [39]
μ (μ_N)	0.840	0.811	–	–	–
$R_{\rm rms}$ (fm)	2.64	2.64	2.65	2.65	2.81 ± 0.14 [40]
R_{12} (fm)	4.11	4.33	4.73	4.63	–
θ_{12} (degree)	72.2	76.3	83.1	80.6	–

the $[j_> \otimes j_<]$ configurations, and, as a result, the transition strength becomes large. Other theoretical approaches [5,17] also take the $[j_> \otimes j_<]$ configurations into account in the model space and agree with our calculation.

The magnetic moment is also sensitive to the structure of the wave function, in particular, to the spin-coupling of the valence neutron and proton. The theoretical calculations [5,17] give large magnetic moments and indicate the dominance of the $S = 1$ channel in the 1^+ ground state, although it has not been measured in experiments. The present calculation yielded $\mu = 0.811\ \mu_N$, as shown in Table 2, which is consistent with other theoretical calculations, $0.834\,\mu_N$ [5] and $0.82\mu_N$ [17]. The $S = 1$ channel dominance in the ^{18}F wave function can be confirmed by the decomposition of the magnetic moment to the orbital angular momentum and spin parts, μ^L and μ^S, as follows:

$$\mu = \left\langle \sum_i g_l^{(i)} \boldsymbol{l}_i \right\rangle + \left\langle \sum_i g_s^{(i)} \boldsymbol{s}_i \right\rangle \equiv \mu^L + \mu^S. \tag{9}$$

In the limit of the pure $S = 1$ channel in the LS-coupling scheme, where the orbital angular momentum part μ^L is identically zero, the spin part becomes exactly half of the sum of the neutron and proton spin g-factors as $\mu = (5.586 - 3.826)/2 = 0.880\ \mu_N$. Our calculation gives the values $\mu^L = 0.090$ and $\mu^S = 0.721$ (μ_N), which are close to the limit values mentioned above, showing the dominance of the $S = 1$ channel in the 1^+ ground state. From this result, we imagine the formation of the spatially localized deuteron-like pair with $S = 1$ and its orbital motion around the ^{16}O (0^+) core with $L = 0$.

As summarized in Table 2, our calculation yields the matter radius $R_{\rm rms} = 2.64$ fm, which is close to the lower limit of the observed radius [40], and the distance R_{12} and the opening angle θ_{12} are calculated as 4.37 fm and 76.3°. We compare these values with those of the ^{6}He (^{4}He+2n system) in which the formation of the di-neutron is expected; many studies have been devoted to discussing the di-neutron correlation [18,41,42]. For example, the theoretical study by Kikuchi et al. [42] reports values of $R_{\rm rms} = 2.46$ fm, $R_{12} = 4.70$ fm, and $\theta_{12} = 67.9°$. Despite the large binding energy in ^{18}F (9.75 MeV) compared to the Borromean nucleus ^{6}He (0.98 MeV), which has a di-neutron-like structure for the valence neutrons, the calculated R_{12} in ^{18}F becomes 4.33 fm and is smaller than that obtained in ^{6}He. Though the opening angle in ^{18}F with the adjusted nucleon–nucleon strength (76.3°) is larger than that of ^{6}He, as shown in Table 2, the angle obtained using the original strength becomes 72.2° and becomes close to the ^{6}He case (67.9°).

From these results, we conclude that (1) the 1^+ ground state of ^{18}F is close to the LS-coupling limit and is dominated by the $S = 1$ channel, and (2) the valence proton and neutron form a deuteron-like pair and its spatial localization is comparable with or even stronger than the so-called di-neutron in ^{6}He.

3.2. *Configuration dependence and deuteron-like correlation*

The purpose of this subsection is to clarify the role of two aspects of the 1^+ state: (1) the change of the coupling scheme from jj-coupling to LS and (2) the localization of the valence nucleons. We consider that the essential ingredients in the model space are the "cross-shell" coupling and the unbound-state (continuum) contributions. For the former part, we separate the contribution of the $[j_> \otimes j_<]$ configuration from the other $(\ell_j)^2$-type configuration and show the difference of the correlation energy. For the latter one, we discuss the spatial localization by including the continuum contribution to the model space. In ^{18}F, the $1s0d$-orbits can be considered as the major shell, since the sd-waves have bound states ($5/2^+$ and $1/2^+$) and a resonant state with a very small decay width ($3/2^+$). The higher nodal components and continuum contributions of sd-waves are also included in this approach using the Gaussian expansion. We take the maximum momentum as $\ell_{\rm mzx} = 6$, and hence the contributions of the pf and higher partial waves are considered as continuum ones, since the poles of the resonant states have a large imaginary part, if they exist, as discussed in the previous subsection.

The contribution of the $[d_{5/2} \otimes d_{3/2}]^1_0$ configuration has been investigated in the sd-shell model picture [6–10]. In Ref. [10], it was pointed out that the LS-coupling scheme enhances the $[d_{5/2} \otimes d_{3/2}]^1_0$ contribution [10]. The change of the coupling scheme from jj- to LS-type induces a non-negligible contribution from the single-particle continua, i.e., the mixing of pf-shell and higher angular momentum configurations leading to the spatially localized deuteron-like pair formation. To illustrate these, we calculate the 1^+ and 0^+ states of ^{18}F by changing the size of the model space and investigate the physical quantities such as correlation energy, magnetic moment, and opening angle.

In the present study, the model space with $\ell_{\rm max} = 6$ gives possible combinations of the angular momenta in the jj-coupling scheme as twenty-four and thirteen for the 1^+ and 0^+ states, respectively. We classify them into six sets of the model space called "CN#", as summarized in Table 3. CN1 to CN3 and CN6 include only $(\ell_j)^2$-type configurations in which the proton and neutron are in the same ℓ_j orbit. Note that the $d_{3/2}$, pf, and higher orbits are unbound, as shown in Table 1; hence, CN3 and CN6 represent the contribution from the single-particle continua of the major shell and higher shells. Since the $d_{3/2}$-wave has a resonant state with a very small decay width, the $0d_{3/2}$-pole contribution become dominant in the $d_{3/2}$-wave.

Unlike the above model space, CN4 includes the $[d_{5/2} \otimes d_{3/2}]$ and $[s_{1/2} \otimes d_{3/2}]$ configurations, which are able to participate in 1^+ states but not in 0^+ states. As shown later, the $[d_{5/2} \otimes d_{3/2}]$ configuration, which we call the "cross-shell configuration" is especially important, while the $[s_{1/2} \otimes d_{3/2}]$ configuration is negligible. Schematic pictures of the $(\ell_j)^2$-type and the cross-shell configurations are shown in Figs. 4(a) and (b), respectively. CN5 includes all possible configurations in addition to CN4 up to $\ell_{\rm max} = 6$ with the cross-shell contributions. In short, CN5 corresponds to the full model space for the 1^+ ($T = 0$) state, while CN6 corresponds to that for the 0^+ ($T = 1$) state.

In Fig. 5, we show the model-space dependence of the correlation energies for 1^+ and 0^+. Here, the correlation energy $E^{0d_{5/2}}_{\rm corr}$ is defined as the difference between the energy of the three-body system $E(J^\pi)$ and the sum of the single-particle energies of the valence proton and neutron $\left(\epsilon^\pi_{n\ell_j} + \epsilon^\nu_{n\ell_j}\right)$ as

$$E^{0d_{5/2}}_{\rm corr}(J^\pi) \equiv \left(\epsilon^\pi_{0d_{5/2}} + \epsilon^\nu_{0d_{5/2}}\right) - E\left(J^\pi\right), \tag{10}$$

where the calculated ground-state energies of ^{17}F $\left(5/2^+\right)$ and ^{17}O $\left(5/2^+\right)$ in Table 1 are adopted as $\epsilon^\pi_{0d_{5/2}}$ and $\epsilon^\nu_{0d_{5/2}}$.

Table 3. Applied configurations to the basis set for ^{18}F.

No.	Name	Partial waves
1	CN1	$(d_{5/2})^2$
2	CN2	"CN1" + $(s_{1/2})^2$
3	CN3	"CN2" + $(d_{3/2})^2$
4	CN4	"CN3" + $(d_{5/2})(d_{3/2})$ + $(s_{1/2})(d_{3/2})$
5	CN5	"CN4" + all possible combinations
6	CN6	All possible $(l_j)^2$ combinations

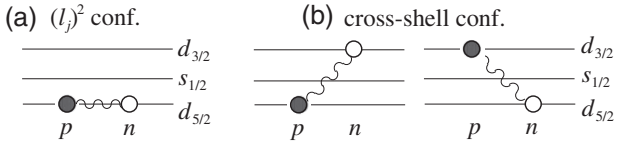

Fig. 4. A schematic figure for (a) $(l_j)^2$-type ($(d_{5/2})^2$) and (b) "cross-shell" ($[d_{5/2} \otimes d_{3/2}]$) configurations of valence nucleons.

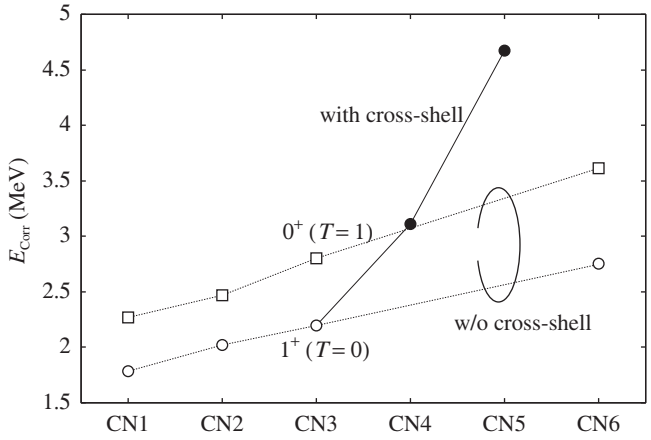

Fig. 5. Model-space dependence of the correlation energies for the 1^+ ($T = 0$) and 0^+($T = 1$) states of ^{18}F. Open circles and squares correspond to the calculations using only the $(\ell_j)^2$-type configurations. The solid circles are for calculations using the cross-shell configurations. The lines are drawn to guide the eyes.

First, to see the difference between the 1^+ and 0^+ states in the same model space, we focus on the results obtained with only the $(\ell_j)^2$-type configurations: CN1, CN2, CN3, and CN6. The correlation energies for both 1^+ and 0^+ increase as the model space becomes larger, and we can find the following two interesting features. One is the similar behavior of the correlation energies for 1^+ and 0^+, and the other is that the correlation energies of the 1^+ states are systematically smaller than those of the 0^+ states, despite the fact that the nuclear force is more attractive in the $T = 0$ channel. To understand these features, we compare the wave functions of the 1^+ and 0^+ states with the decomposition to each component. As seen from Fig. 6, the compositions of the 1^+ wave function obtained by the CN2, CN3, and CN6 model spaces are quite similar to those of the 0^+ states, which has the nature of an ordinary $T = 1$ pairing. As the model space is enlarged, the occupation probability of the orbits above the Fermi level ($d_{5/2}$), in particular those close to or just above the Fermi level, increases. Consequently, the $(s_{1/2})^2$ configuration becomes the second leading component for both the 1^+ and 0^+ states in CN6 model space. Since the compositions of the wave functions are similar to each other,

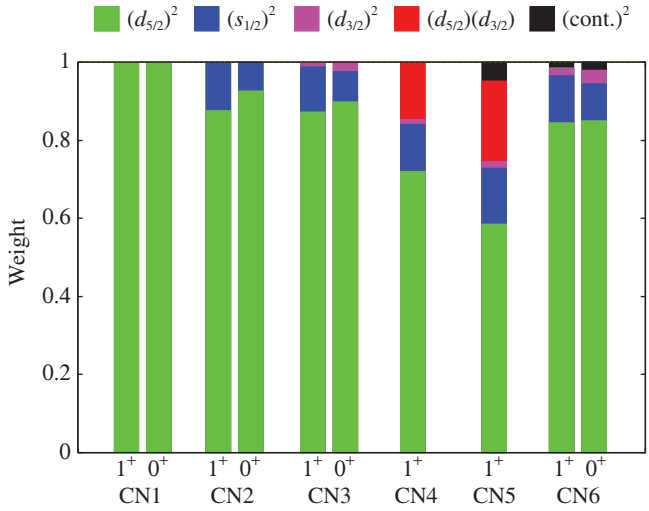

Fig. 6. Model-space dependence of the composition of the 1^+- and 0^+-state wave functions. "(cont.)^2" shows the components of higher partial waves above the sd-shell.

we can understand that the 1^+ and 0^+ states show similar behavior for the correlation energy, and the difference in the correlation energy mainly comes from the potential energy between the valence proton and neutron. For example, the difference in the correlation energy at CN6 is

$$\left|E_{\rm corr}^{0d_{5/2}}(1^+) - E_{\rm corr}^{0d_{5/2}}(0^+)\right| = |2.76 - 3.61| = 0.85({\rm MeV}),$$

and we see that it is very close to the difference in the expectation value of the nucleon–nucleon potential as

$$\left|\left\langle \hat{V}_{12}\right\rangle_{1^+}^{\rm CN6} - \left\langle \hat{V}_{12}\right\rangle_{0^+}^{\rm CN6}\right| = |(-3.76) - (-4.87)| = 1.11\ ({\rm MeV}).$$

Considering the above discussion, the weakness of the potential attraction for the $J = 1^+$ proton–neutron pair compared to the $J = 0^+$ pair is easily understood, as already discussed by many authors [4,11]. Namely, as is well known for the ordinary $T = 1$ pairing, a $J = 0^+$ nucleon pair occupying the same j orbit can maximize the spatial overlap and gains a large potential attraction. On the other hand, a $J = 1^+(T = 0)$ nucleon pair occupying the same j orbit cannot, and does not gain strong attraction from the potential despite the stronger nuclear force in the $T = 0$ channel.

The change in the coupling scheme to the LS-coupling brings the "cross-shell configuration" to the basis set and also to the behavior of the correlation energy, because it enables the formation of a $J = 1$ nucleon pair coupled to $L = 0$ and $S = 1$, which maximizes the spatial overlap. This can be confirmed with the results on the solid line of Fig. 5. In the CN4 result, the correlation energy of the 1^+ state is increased by 0.91 MeV $\left(E_{\rm corr}^{0d_{5/2}} = 3.11\ {\rm MeV}\right)$ compared to CN3 and is as large as that of the 0^+ state in CN6. From Fig. 6, we see that the composition of the wave function is also considerably changed in CN4, and the $\left[d_{5/2} \otimes d_{3/2}\right]_0^1$ configuration becomes the second leading component. Here, we note that the amount of the $\left[s_{1/2} \otimes d_{3/2}\right]_0^1$ configuration is negligible (less than 0.01), and then conclude that the $\left[d_{5/2} \otimes d_{3/2}\right]_0^1$ configuration is the main component in the change of the structure of the wave function to LS-coupling and that it triggers the $T = 0$ pair correlation. This structural-change including the cross-shell configuration is clearly observed in the magnetic moment, as discussed later.

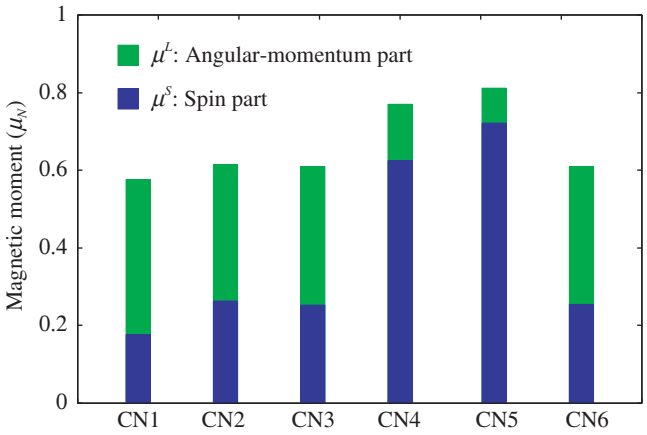

Fig. 7. Model-space dependence of magnetic moment for ^{18}F(1^+).

It is also interesting and important to note that the contribution from the single-particle continua (s.p.c.), i.e., pf and higher partial waves, is also increased accompanied by the cross-shell configuration. Compared to the result without the cross-shell (CN6), the amount of the s.p.c. configuration is considerably increased in CN5. The "(cont.)^2" contribution in Fig. 6, which is the rest of the components in the wave function $(d_{5/2})^2$, $(1_{2/2})^2$, $(d_{3/2})^2$, and $(d_{5/2})(d_{3/2})$ subtracted from the wave function, becomes three times larger in the 1^+ state from CN6 to CN5, 0.016 to 0.048, as shown in Fig. 6. Also, compared to that of 0^+ with CN6 (0.022), the 1^+ state with CN5 is 1.5 times larger. Therefore, the continuum contribution is enhanced by the presence of the cross-shell configurations. Owing to this contribution from continua, the correlation energy is further increased by 1.56 MeV from the CN4 result and is very large $\left(E_{\rm corr}^{0d_{5/2}}(1^+) = 4.67\,{\rm MeV}\right)$ in CN5.

The magnetic moment provides interesting information on the wave function. Figure 7 shows the configuration dependence of the magnetic moment with decomposition into the orbital angular momentum and spin parts defined in Eq. (9). For the $(\ell_j)^2$-type configurations (CN1, CN2, CN3, and CN6), the calculated magnetic moments are relatively small and are approximately equal to $0.6\,\mu_N$. The orbital part μ^L is systematically larger than the spin part μ^S. Hence, the wave function can be considered as a mixture of the $S = 1$ and 0 channels. Once the cross-shell configuration in the major shell is added (CN4), the magnetic moment suddenly increases to 0.770 μ_N, and the roles of the angular momentum part μ^L and spin part μ^S are drastically interchanged. μ^S increases from 0.253 to 0.625 (μ_N), while μ^L decreases from 0.356 to 0.145 (μ_N). The large contribution of the spin part μ^S at CN4 is clear evidence of the change of the wave function from the jj-coupling to LS-coupling scheme with $S = 1$. The s.p.c. contribution brings about further enhancement of the $S = 1$ dominance, as shown in the CN5 case; see Fig. 7. The magnetic moment increases to 0.811 μ_N, and its decomposition becomes $\mu^L = 0.090$ and $\mu^S = 0.721$ (μ_N).

From the viewpoint of the spatial correlation of the proton and neutron, the contribution from the s.p.c. is essential. As is known for the $T = 1$ pair cases [18], admixture of the even- and odd-parity single-particle states is necessary to form a spatially correlated and localized pair. From CN1 to CN4, only the even-parity basis functions are included, and the opening angles of these cases become 90°. The contribution from the s.p.c. configurations reduces the opening angles in CN5 and CN6. For the CN6 case, the calculated angles of the 1^+ and 0^+ states are $\theta_{12} = 83.3°$ and 80.6°, respectively. The 1^+ state in CN5 has the smallest opening angle, $\theta_{12} = 76.3°$. This is consistent with the results for the correlation energy and the contribution from the s.p.c. configurations in CN5 for 1^+, where

both the quantities become largest. This is a reminder that the large contribution from the s.p.c. in CN5 is triggered by the cross-shell configurations of the d-wave and also the higher partial waves, and our theoretical model properly takes the single-particle continua into account by the use of the Gaussian expansion method. Therefore, we conclude that the proper treatment of the s.p.c. and the inclusion of the the cross-shell configuration are essential for the description of the spatially localized deuteron-like pair.

To summarize so far, the proton and neutron correlation in ^{18}F can be characterized by the following three aspects. First, without the cross-shell configuration, the coupling scheme and the composition of the wave function are essentially the same in the 1^+ and 0^+ states. Second, once we include the cross-shell configuration in the 1^+ state, the correlation energy becomes comparable to that of the 0^+ state owing to the $S = 1$ proton–neutron pair formation. The analysis of the magnetic moment shows a drastic change from jj-coupling to LS-coupling. Finally, the continuum contribution makes the correlation energy much larger than the 0^+ state. It also induces spatial localization of the valence nucleons, as shown in the calculation of the opening angle of the valence nucleons.

3.3. *Spin–orbit-interaction dependence*

In the previous subsection, we showed that the cross-shell configuration plays a crucial role in the correlation energy of the $T = 0$ nucleon pair and in the spatially localized formation of the deuteron-like pair due to the LS-coupling scheme dominance. Energetically, the cross-shell in the major shell, $[d_{5/2} \otimes d_{3/2}]^1_0$, mainly contributes to the correlation energy in the $T = 0$ channel pair. Since the cross-shell component is formed by the coupling of two nucleons as the spin–orbit partners, i.e., $d_{5/2}$ and $d_{3/2}$, the correlation strength should depend on the magnitude of the spin–orbit splitting. In order to see the effect of the spin–orbit splitting on the correlation energy and the composition of the wave functions, we vary the strength of the spin–orbit potential by multiplying a factor β_{LS} by $\hat{v}_i^{LS}$ in Eq. (6) as

$$\hat{v}_i^{LS} \Longrightarrow \beta_{LS} \cdot \hat{v}_i^{LS}, \tag{11}$$

where β_{LS} is varied from 0 to 2.0. In the case of the original strength $\beta_{LS} = 1.0$, the energy splitting between $0d_{5/2}$ and $0d_{3/2}$ is approximately 5 MeV, as shown in Table 1.

The correlation energies of the 1^+ and 0^+ states and the composition of the wave function as a function of β_{LS} are shown in Figs. 8(a) and (b). First, we focus on the larger spin–orbit splitting cases by increasing β_{LS} from 1.0 to 2.0. As the spin–orbit strength increases, the $d_{5/2}$-orbit is bound more deeply and become dominant in the components of the wave function. As a result, the amount of the $(d_{5/2})^2$ configuration gets larger in both the 1^+ and 0^+ states. In particular, in the 0^+ state, the dominance of the $(d_{5/2})^2$ component is prominent, and other contributions are negligible in the region of $\beta_{LS} \geq 1.5$. At $\beta_{LS} = 2.0$, the $(d_{5/2})^2$ configuration amounts to 0.97 and the correlation energy is $E_{\rm corr}^{0d_{5/2}}\left(0^+\right) = 3.22$ MeV. On the other hand, other configurations, in particular the cross-shell configuration, are non-negligible in the 1^+ state even at $\beta_{LS} = 2.0$. The correlation energy increases as $E_{\rm corr}^{0d_{5/2}}\left(1^+\right) = 3.56$ MeV and is larger than the 0^+ state. This shows the importance of the cross-shell configuration to the $T = 0$ pair correlation. We also calculated the magnetic moment of the 1^+ state at $\beta_{LS} = 2.0$, obtained as $\mu = 0.691\ \mu_N$, and the spin-part dominance is confirmed by the results $\mu^L = 0.248$ and $\mu^S = 0.443\ (\mu_N)$. This is more evidence of the importance of the cross-shell configuration that gives rise to the $L = 0$ and $S = 1$ pair formation.

Next, we focus on the smaller spin–orbit splitting cases by decreasing β_{LS} from 1.0 to 0. In the present $^{16}\mathrm{O} + N$ potential model, the $0d_{5/2}$ and $1s_{1/2}$ orbits are degenerated at $\beta_{LS} = 0.7$, and the

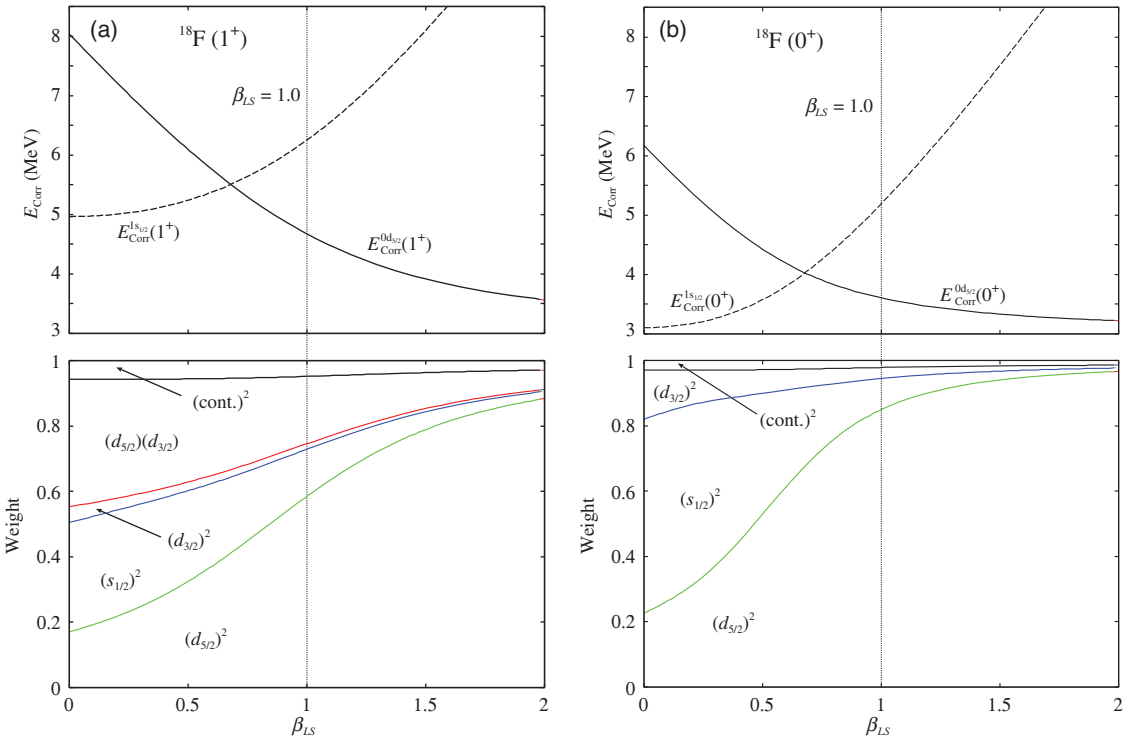

Fig. 8. Upper panels: β_{LS} dependence on the correlation energy for ^{18}F(1^+) and ^{18}F(0^+). Lower panels: the weights of the wave function for the 1^+ and 0^+ states are shown.

$1s_{1/2}$ orbit becomes the lowest one for $\beta_{LS} < 0.7$. Therefore, we also calculated the correlation energies defined with respect to the $\left(1s_{1/2}\right)^2$ configuration for the 1^+ and 0^+ states as

$$E^{1s_{1/2}}_{\rm corr}\left(J^\pi\right) \equiv \left(\epsilon^\pi_{1s_{1/2}} + \epsilon^\nu_{1s_{1/2}}\right) - E\left(J^\pi\right). \tag{12}$$

As β_{LS} decreases, the leading configuration changes from $(d_{5/2})^2$ to others. For the 0^+ state, the $(s_{1/2})^2$ configuration takes over the $(d_{5/2})^2$ configuration, as naturally expected. On the other hand, in the 1^+ state, the $(d_{5/2})(d_{3/2})$ and $(s_{1/2})^2$ configurations are always comparable, and the $(d_{5/2})(d_{3/2})$ configuration is even larger. At $\beta_{LS} = 0.7$, where the $0d_{5/2}$ and $1s_{1/2}$ orbits degenerate, the correlation energies of the 1^+ and 0^+ states become maximum as $E_{\rm corr}\left(1^+\right) = 5.44$ and $E_{\rm corr}\left(0^+\right) = 3.99$ MeV.

In the limit of $\beta_{LS} = 0$, the wave function of the valence proton and neutron is identical to the LS-coupling. In this limit, the relative ratio of the components of $(d_{5/2})^2$, $(d_{3/2})^2$, $(d_{5/2})(d_{3/2})$ can be obtained from the transformation of the LS-coupling wave function to the jj-coupling one as follows:

$$\left|\,[L \otimes S]^J_T\,\right\rangle = \sum_{j_\pi\, j_\nu} \hat{L}\,\hat{S}\,\hat{j}_\pi\,\hat{j}_\nu \begin{Bmatrix} \ell_\pi & 1/2 & j_\pi \\ \ell_\nu & 1/2 & j_\nu \\ L & S & J \end{Bmatrix} \left|\,[j_\pi \otimes j_\nu]^J_T\,\right\rangle, \tag{13}$$

where $\ell_\pi = \ell_\nu = 2$. For the 1^+ state, $(L, S, J, T) = (0, 1, 1, 0)$, the exact relative ratio of the d-wave components is given as $(d_{5/2})^2 : (d_{3/2})^2 : (d_{5/2})(d_{3/2}) = 7 : 2 : 16$ from the Clebsch–Gordan coefficients in Eq. (13). In our numerical calculation, as shown in the lower panel of Fig. 8(a), the ratio of components in ^{18}F(1^+) with $\beta_{LS} = 0$ becomes $7 : 2.0001 : 15.9991$, which is almost the same

as the exact ratio. Furthermore, the magnetic moment becomes $\mu = 0.880\ \mu_N$ and is equal to the average of the neutron and proton spin g-factors. For the 0^+ state, $(L, S, J, T) = (0, 0, 0, 1)$, the exact ratio of the components becomes $(d_{5/2})^2 : (d_{3/2})^2 = 3 : 2$. The calculated components in the ^{18}F(0^+) wave function give the ratio as $3 : 2.000\,0004$, as shown in the lower panel of Fig. 8(b).

The symmetry of the valence particles affects the contribution of the cross-shell component ($[d_{5/2} \otimes d_{3/2}]$). In our calculation with $\beta = 0.0$, where the spin–orbit splitting vanishes and restores the symmetry, the contribution of the cross-shell component becomes 0.39. The large contribution of the cross-shell component has been shown in the traditional sd-shell model approaches [6,8]. Kuo [6] showed that the $(d_{5/2})(d_{3/2})$ component in the 1^+ state was 0.40, and Rolfs [8] followed the result with almost the same contribution, 0.44. For $\beta = 1.0$, the cross-shell component of our calculation is 0.21 and is smaller than the $\beta = 0.0$ case. The change from $\beta = 0.0$ to 1.0 can be considered as a consequence of the presence of the spin–orbit splitting breaking the SU(3) symmetry of the valence particles. This change has been discussed qualitatively in the sd-shell model space [10]. Kulkarni showed that the cross-shell component without the spin–orbit splitting is 0.55 and is reduced to 0.25 by introducing the splitting. Another shell model approach [9] with a $2p$ and $4p2h$ mixing approach shows a smaller contribution of the cross-shell component of 0.24. Our calculation is similar to these two results, and, of course, it depends on the choice of the nucleon–nucleon interaction.

4. Summary and discussion

We investigated the $T = 0$ proton and neutron correlation in ^{18}F using the COSM approach combined with the Gaussian expansion method. With an adjustment of the Minnesota nucleon–nucleon potential, the observed $T = 0$ and $T = 1$ states of ^{18}F are reasonably described. By the decomposition of the magnetic moment into the orbital and spin parts, the spin-part contribution is found to be dominant and close to the sum of the proton and neutron g-factors. This leads to a picture in which two valence nucleons in the ground state are coupled to an $L = 0$ and $S = 1$ pair in the LS-coupling scheme. Furthermore, it is shown that the opening angle between the valence nucleons is comparable to that of ^{6}He, which means the formation of a spatially correlated deuteron-like pair.

To understand the pair formation mechanism, we have performed the analysis by changing the size of the model space. With only the $\left(\ell_j\right)^2$-type configurations, the correlation energy of the 1^+ state is smaller than that of the 0^+ state. The change of the coupling scheme of the valence nucleons from jj- to LS-coupling induces an increase in the cross-shell configuration such as $[d_{5/2} \otimes d_{3/2}]$, and the situation also changes dramatically, as can be clearly seen in the decomposition of the magnetic moment. As a result, the spatial overlap of the valence nucleons is maximized, leading to the large correlation energy of the 1^+ state.

The continuum contribution is the other important ingredient for the neutron–proton correlation, which gives rise to the spatial localization of the proton and neutron. This effect has been discussed in Refs. [18,43]. We have found that a similar phenomenon occurs in the $T = 0$ channel.

We also discussed the effect of the spin–orbit potential of the core nucleus by changing its overall strength from zero to twice the normal strength. As the strength increases, all components except for $(d_{5/2})^2$ vanish as negligible from the wave functions in the 0^+ state. However, even in such an extreme case, the cross-shell configuration still remains in the 1^+ wave function.

For future work, it is necessary to perform systematic studies on other nuclei in the core $+p$+n model space and investigate the dependence of the available valence orbits on the coupling scheme of the wave function of the valence nucleons.

Acknowledgements

The authors would like to thank the members of the nuclear theory group in Hokkaido University for their kind interest and discussions. One of the authors (M.K.) acknowledges support by Grants-in-Aid for Scientific Research on Innovative Areas from MEXT (Grant No. 2404:24105008) and JSPS KAKENHI Grant 563 No. 25400240.

References

[1] J. A. Evans, G. G. Dussel, E. E. Maqueda, and R. P. J. Perazzo, Nucl. Phys. A **367**, 77 (1981).
[2] A. Poves and G. Martines-Pinedo, Phys. Lett. B **430**, 203 (1998).
[3] A. L. Goodman, Phys. Rev. C **60**, 014311 (1999).
[4] H. Sagawa, Y. Tanimura, and K. Hagino, Phys. Rev. C **87**, 034310 (2013).
[5] Y. Tanimura, H. Sagawa, and K. Hagino, Prog. Theor. Exp. Phys. **2014**, 053D02 (2014).
[6] T. T. S. Kuo and G. E. Brown, Nucl. Phys. **85**, 40 (1966).
[7] A. Arima, S. Cohen, R. D. Lawson, and M. H. Macfarlane, Nucl. Phys. A **108**, 94 (1968).
[8] C. Rolfs, W. E. Kieser, R. E. Azuma, and A. E. Litherland, Nucl. Phys. A **199**, 274 (1973).
[9] T. Sakuda, S. Nagata, and F. Nemoto, Prog. Theor. Phys. **56**, 1126 (1976).
[10] D. R. Kulkarni and S. P. Pandya, Nuovo Cimento B **60**, 199 (1969).
[11] G. F. Bertsch and Y. Luo, Phys. Rev. C **81**, 064320 (2010).
[12] A. Gezerlis, G. F. Bertsch, and Y. L. Luo, Phys. Rev. Lett. **106**, 252502 (2011).
[13] K. Hagino, H. Sagawa, J. Carbonell, and P. Schuck, Phys. Rev. Lett. **99**, 022506 (2007).
[14] N. T. Zinner and A. S. Jensen, Phys. Rev. Lett. **101**, 179201 (2008).
[15] K. Hagino, H. Sagawa, J. Carbonell, and P. Schuck, Phys. Rev. Lett. **101**, 179202 (2008).
[16] A. F. Lisetskiy, R. V. Jolos, N. Pietralla, and P. von Brentano, Phys. Rev. C **60**, 064310 (1999).
[17] Y. Kanada-En'yo and F. Kobayashi, Phys. Rev. C **90**, 054332 (2014).
[18] K. Hagino and H. Sagawa, Phys. Rev. C **72**, 044321 (2005).
[19] Y. Suzuki and K. Ikeda, Phys. Rev. C **38**, 410 (1988).
[20] E. Hiyama, Y. Kino, and M. Kamimura, Prog. Part. Nucl. Phys. **51**, 223 (2003).
[21] S. Aoyama, T. Myo, K. Katō, and K. Ikeda, Prog. Theor. Phys. **116**, 1 (2006).
[22] T. Myo, Y. Kikuchi, H. Masui, and K. Katō, Prog. Part. Nucl. Phys. **79**, 1 (2014).
[23] H. Masui, K. Katō, and K. Ikeda, Phys. Rev. C **75**, 034316 (2007).
[24] N. Michel, W. Nazarewicz, M. Płoszajczak, and K. Bennaceur, Phys. Rev. Lett. **89**, 042502 (2002).
[25] R. Id Betan, R. J. Liotta, N. Sandulescu, and T. Vertse, Phys. Rev. Lett. **89**, 042501 (2002).
[26] N. Michel, W. Nazarewicz, M. Płoszajczak, and J. Okołowicz, Phys. Rev. C **67**, 054311 (2003).
[27] N. Michel, W. Nazarewicz, and M. Płoszajczak, Phys. Rev. C **70**, 064313 (2004).
[28] H. Masui, K. Katō, N. Michel, and M. Płoszajczak, Phys. Rev. C **89**, 044317 (2014).
[29] H. Masui, K. Katō, and K. Ikeda, Phys. Rev. C **73**, 034318 (2006).
[30] H. Masui, K. Katō, and K. Ikeda, Eur. Phys. J. A **42**, 535 (2009).
[31] H. Masui, K. Katō, and K. Ikeda, Nucl. Phys. A **895**, 1 (2012).
[32] T. Kaneko, M. LeMere, and Y. C. Tang, Phys. Rev. C **44**, 1588 (1991).
[33] S. Saito, Prog, Theor. Phys. Suppl. **62**, 11 (1977).
[34] V. I. Kukulin, V. M. Krasnopol'sky, V. T. Voronchev, and P. B. Sazonov, Nucl. Phys. A **417**, 128 (1984).
[35] Y. K. Ho, Phys. Rep. **99**, 1 (1983).
[36] F. Ajzenberg-Selove, Nucl. Phys. A **460**, 1 (1986).
[37] D. R. Thompson, M. LeMere, and Y. C. Tang, Nucl. Phys. A **286**, 53 (1977).
[38] F. Ajzenberg-Selove, Nucl. Phys. A **475**, 1 (1987).
[39] National Nuclear Data Center, *Chart of nuclides* (National Nuclear Data Center, New York, n.d.). (Available at: http://www.nndc.bnl.gov/chart/, date last accessed April 11, 2014).
[40] A. Ozawa, T. Suzuki, and I. Tanihata, Nucl. Phys. A **693**, 32 (2001).
[41] M. V. Zhukov, B. V. Danilin, D. V. Fedorov, J. M. Bang, I. J. Thompson, and J. S. Vaagen, Phys. Rep. **231**, 151 (1993).
[42] Y. Kikuchi, K. Katō, T. Myo, M. Takashina, and K. Ikeda, Phys. Rev. C **81**, 044308 (2010).
[43] S. Aoyama, S. Mukai, K. Katō, and K. Ikeda, Prog. Theor. Phys. **93**, 99 (1995).